Article

Not peer-reviewed version

A New Generation of Hydrogen Fueled Hybrid Propulsion Systems for the Urban Mobility of the Future

Ivan Arsie , Michele Battistoni , Pier Paolo Brancaleoni , Roberto Cipollone , Enrico Corti , Davide Di Battista , Federico Millo , Alessio Occhicone , Benedetta Peiretti Paradisi * , Luciano Rolando * , Jacopo Zembi

Posted Date: 20 November 2023

doi: 10.20944/preprints202311.1191.v1

Keywords: Hydrogen; H2-ICE; Decarbonization; Public transport

Article

A New Generation of Hydrogen Fueled Hybrid Propulsion Systems for the Urban Mobility of the Future

Ivan Arsie [1], Michele Battistoni [2], Pier Paolo Brancaleoni [4], Roberto Cipollone [3], Enrico Corti [4], Davide Di Battista [3], Federico Millo [5,*], Alessio Occhicone [1], Benedetta Peiretti Paradisi [5,*], Luciano Rolando [5,*] and Jacopo Zembi [2]

[1] Università degli Studi di Napoli Parthenope, Italy
[2] Università degli Studi di Perugia, Italy
[3] Università dell'Aquila, Italy
[4] Università degli studi di Bologna, Italy
[5] Politecnico di Torino, Italy
* Correspondence: benedetta.peiretti@polito.it (B.P.P.); luciano.rolando@polito.it (L.R.)

Abstract: The H2-ICE project aims at developing, through numerical simulation, a new generation of hybrid powertrains featuring a hydrogen fueled Internal Combustion Engine (ICE) suitable for 12-meter urban buses, in order to provide a reliable and cost-effective solution for the abatement of both CO_2 and criteria pollutant emissions. The full exploitation of the potential of such a traction system requires a substantial enhancement of the state of the art since several issues have to be addressed. In particular, the choice of the more suitable fuel injection system, as well as the control of the combustion process, are extremely challenging. Firstly, a high-fidelity 3D-CFD model will be exploited to analyze the in-cylinder H2 fuel injection through supersonic flows. Then, after the optimization of the injection and combustion process, a 1D model of the whole engine system will be built and calibrated allowing the identification of a "sweet spot", in the ultra-lean combustion region, characterized by extremely low NOx emissions and, at the same time, high combustion efficiencies. Moreover, to further enhance the engine efficiency well above 40 %, different Waste Heat Recovery (WHR) systems will be carefully scrutinized, including both Organic Rankine Cycle (ORC)-based recovery units as well as electric turbo-compounding. A Selective Catalytic Reduction (SCR) aftertreatment system will be developed to further reduce NOx emissions to near-zero levels. Finally, a dedicated torque-based control strategy for the ICE coupled with the Energy Management Systems (EMS) of the hybrid powertrain, both optimized by exploiting Vehicle-To-Everything (V2X) connection, allow targeting an H2 consumption of 0.1 kg/km. Technologies developed in the H2-ICE project will enhance the know-how necessary to design and build engines and after-treatment systems for the efficient exploitation of H2 as a fuel, as well as for their integration into hybrid powertrains.

Keywords: hydrogen; H2-ICE; decarbonization; public transport

1. Introduction

In the context of decarbonization of the transportation sector, regulators are imposing increasingly stringent limitations in terms of CO_2 emissions, and the European Commission has declared its ambition to reach zero net Green House Gas (GHG) emissions by 2050 [1]. As a matter of fact, 35% of the worldwide energy consumption is due to the transportation sector [2] and in 2020 road transport constituted 77% of all European Union (EU) transport GHG emissions [3]. In this sector, lorries, buses, and coaches are responsible for more than a quarter of GHG emissions in the EU (i.e., over 6% of total European GHG emissions) [4]. To mitigate this contribution, stronger CO_2 emissions standards have been set by the EU for Heavy Duty Vehicles (HDV), including smaller

trucks and urban or suburban buses. The proposal establishes a 90% decrease in CO_2 emissions per km from new HDV by 2040 (compared to a mid-2019 to mid-2020 baseline) with intermediate targets for 2030 (45%) and 2035 (65%) [5].

In this framework, synergetic exploitation of decarbonized energy carriers and powertrain electrification could shift the public transportation fleets towards more sustainable mobility, compliant with current legislation targets. On the one hand, Battery Electric Vehicles (BEVs) may represent a promising alternative to improve the air quality of highly congested urban areas and to decarbonize the Light Duty Vehicles (LDVs) sector [6]. On the other hand, due to the limited specific energy of chemical batteries, BEVs are still not considered suitable for applications where the payload or the operative range are the main constraints (e.g., commercial vehicles or buses), requiring high initial costs and large size batteries [7,8]. Among the possible alternatives for the HDV sector, the exploitation of hydrogen as an alternative fuel could play a key role in the EU energy transition [9], ensuring zero carbon-based emissions (e.g., CO, CO_2, and soot), and high energy efficiency. In addition, the production path of hydrogen could rely on a wide variety of available technologies and energy resources, many of which are renewables and/or have low carbon impact, strengthening the argument for hydrogen as a long-term sustainable energy vector to fuel the future [10]. In the context of the public urban transportation sector, hydrogen has been already exploited in Fuel Cells Electric Vehicles (FCEV), demonstrating significant advantages with respect to BEVs, both in terms of weight reduction and range increase, with lower refueling time [11,12]. Moreover, using hydrogen as a fuel to power Internal Combustion Engines (ICEs) could add further benefits with respect to Fuel Cell (FC) technology, such as a great tolerance to fuel contamination, significant cost savings (up to one order of magnitude) and the possible exploitation of existing production lines, due to familiar technologies and parts with current Internal Combustion Engine Vehicle (ICEV) [13]. Furthermore, one of the main concerns regarding hydrogen vehicles is the need for new infrastructures for hydrogen distribution and refueling, while in the case of urban buses a quite limited range is typically requested, and tank refueling is not an issue, since it is possible for captive fleets to centralize the fuel station.

Despite the great potential of H2 as a fuel for ICEs in public transport, in the last two decades, it has been implemented in few prototypes [14,15] and real bus fleets, such as in the two demonstration projects HyFLEET:CUTE [16] and SunLine Cleen Fleet [17]. In particular, HyFLEET project involved the operation of 47 hydrogen-powered buses in regular public transport service in 10 cities on three continents, from 2006 to 2009, testing on 15 buses two different types of H2-ICEs (naturally aspirated or turbocharged). In addition, SunLine Cleen Fleet tested a prototype hybrid H2-ICE bus in California for three years (2006-2008). The outcomes of both projects have shown that hydrogen can be a low or even emission-free transport fuel, implementing today's technology. Nevertheless, some issues remain unresolved, such as the performance of the fuel injectors, the turbocharged operation, and the control of the engine management system. Moreover, a rising interest has been growing recently for the development of a new generation of ICEs designed to be operated at high boost levels with ultra-lean mixtures, thus simultaneously achieving extremely low NOx emissions (< 0.05 g/kWh), along with high efficiency values (> 42%) at lambda>2 [18–20]. A further enhancement could be obtained through the synergic combination with hybrid propulsion technologies, particularly suitable for urban bus applications, for which series hybrid could significantly benefit from energy recovery through regenerative braking, as well as from a substantial downsizing of the ICE, being vehicle acceleration performance decoupled from engine power output [21].

In this context, the present research project, so-called H2-ICE project, aims to develop an innovative hybrid H2-fueled powertrain for urban bus application, giving insights into the current knowledge gap for H2 exploitation in ICE. Specifically, the approach adopted for the H2-ICE project consists, at first, of defining the use case scenarios for the targeted application (i.e. 12 mt urban bus) and emission and fuel consumption targets to be met. This essential preliminary step allows to specify the boundary conditions and the requirements delineating the development scope of the main vehicle subsystems. Then, in a second step, the H2 engine and its subsystems will be developed and optimized, starting from a state-of-the-art diesel engine. Afterward, inc a third step, the engine and

 doi:10.20944/preprints202311.1191.v1

its subsystems are tested and modelled to be integrated into a virtual high-fidelity simulation model and the energy management system will be developed exploiting Vehicle-To-Everything (V2X) connectivity. Finally, the virtual demo vehicle will be evaluated to demonstrate its capabilities in real-world driving conditions. The present work is focused on the development phase of the engine and its subsystems and is then organized as follows: Section 2 provides an overview of the project, with the case study description, a discussion of the challenging issues to be addressed, the overall fixed targets, and the hybrid powertrain technical specifications. Afterward, Section 3 describes the analysis of the suitable combustion and fuel injection system, Section 4 the WHR System together with the aftertreatment technologies needed, and Section 5 the Engine and Powertrain Management strategy. Finally, the actual findings and future steps of the project are presented in Section 6.

2. H2ICE project overview

The H2ICE project aims to enhance the know-how necessary to design and build engine and after-treatment systems for the efficient exploitation of H2 as a fuel and for their integration into a hybrid powertrain, for a series urban bus. In particular, the full exploitation of the potential of such a powertrain requires a substantial enhancement of the state of the art, since several challenging issues have to be addressed. At first, the combination of high efficiency, low emissions, high specific power output, and durability are not all currently achievable in one H2 combustion concept. Starting from fuel injection, Port Fuel Injection (PFI) and Direct Injection (DI) are the two main considered and tested options [22,23]. On the one hand, PFI part load efficiency can be quite high with ultra-low NOx emissions, thanks to the possibility of ultra-lean operation allowed by the extremely high flame propagation and wide flammability limits characteristics of H2 combustion. However, the specific work output is typically limited to 14 bar Brake Mean Effective Pressure (BMEP) due to the low H2 density, even in highly boosted engines. On the other hand, DI engines have proved to be capable of achieving power densities 15% higher than PFI, while offering high efficiencies thanks to possible charge stratification at part load, with a lower risk of abnormal combustion [24]. Nevertheless, DI injectors still have to prove their durability as well as their operability with extra high flow rates, typical of gaseous fuel such as H2. Moreover, the exploitation of fully optimized fuel injection strategies requires high injection pressures, typically above 100 bar, limiting H2 storage options [25]. Indeed, liquid H2 could be stored onboard in cryogenic tanks at a pressure of 16 bar, providing injection pressures onboard, or high-pressure tanks could be exploited to store gaseous hydrogen onboard with a working pressure generally ranging from 350 to 700 bar, but then the full tank capacity may not be utilized. As far as H2 combustion is concerned, the same properties that make H2 a suitable fuel for ICEs can be responsible for high risks of abnormal combustion phenomena: the wide flammability limits, the low ignition energy and the high flame speeds can, as a matter of fact, result in combustion anomalies such as surface ignition, backfiring, preignition and knock [26]. Although significant signs of progress were made in improving computational tools for modeling and understanding mixture formation and combustion in H2 engines [27,28], the numerical simulation of mixture formation for DI H2 engines remains extremely challenging, because of the high-velocity gas jet, leading to a complex structure of shock waves and making charge stratification quite hard to be achieved. Moreover, as far as combustion modeling is concerned, there is a shortage of data on H2 ignition and combustion properties at engine conditions of pressure and temperature, and there has been little progress in extending the current dataset. Furthermore, both advanced WHR systems [29] and an innovative Selective Catalytic Reduction (SCR) aftertreatment system, based on hydrogen as the reductant element, [30] need to be synergically developed to exploit the high exhaust gas enthalpy available and achieve near-zero tailpipe NOx. In addition, the use of H2 as a reducing fluid needs proper catalyst preparation, testing and modelling to be then coupled to the engine. Finally, the elaboration of control strategies for the synergic operation of the developed WHR and H2-SCR aftertreatment systems and the exploitation of look-ahead information from V2X connectivity for the Energy Management System (EMS) of hybrid powertrains is just at the beginning of its exploitation [31]. The H2-ICE project thus aims not only to develop an innovative hybrid H2-

Preprints (www.preprints.org) | NOT PEER-REVIEWED | Posted: 20 November 2023 doi:10.20944/preprints202311.1191.v1

fueled powertrain and related technological opportunities but also to contribute to filling the knowledge gap for H2 exploitation in ICEs, as summarized in Figure 1.

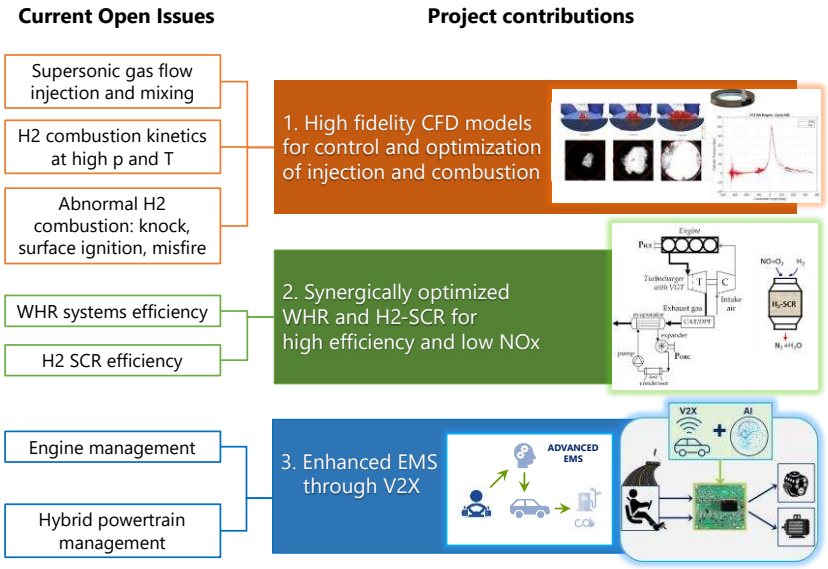

Figure 1. H2-ICE project state-of-the-art enhancements.

Case study

First of all, the H2-ICE project defines the use case scenarios for the targeted application and emission and fuel consumption targets to be met, allowing to specify the boundary conditions and the requirements delineating the development scope of the main vehicle subsystems. The vehicle developed is a 12 mt urban bus with a series hybrid architecture, featuring an H2-ICE derived from a state-of-the-art diesel engine and a tractive electric motor as power units. Vehicle technical specifications and target settings are then listed in Table 1.

Table 1. Hybrid bus specifications and target settings.

Vehicle length	12 m
Curb weight	12 ton
Fully loaded weight	18 ton
Passenger capacity	90
Road Load @ 50 km/h	16 kW
Road Load @ 80 km/h	43 kW
Road Load @ 100 km/h	74 kW

In addition, Table 2 presents the overall targets of the project.

Table 2. H2-ICE targets for vehicle and engine efficiency and NOx emissions.

Vehicle performance	**Max Speed**	65 km/h
	Min Acceleration	1.1 m/s^2
	Max Gradeability @Full Load	14%
Vehicle and engine efficiency	**Specific power**	40 kW/dm^3
	ICE efficiency	42 % peak efficiency
		35 % part load efficiency
	Fuel consumption	0.1 kg/km
Emissions	**NOx tailpipe**	<0.05 g/kWh
Auxiliaries	**WHR system efficiency**	>4%
	eTurbo efficiency	>4%

Preprints (www.preprints.org) | NOT PEER-REVIEWED | Posted: 20 November 2023 doi:10.20944/preprints202311.1191.v1

Both regulatory driving cycles and real-world mission profiles will be taken into account in the design of the hybrid traction system. In particular, three different mission profiles, representative of a typical urban bus operation will be considered, the speed profiles are represented in Figure 2 and their specifications are listed in Table 3.

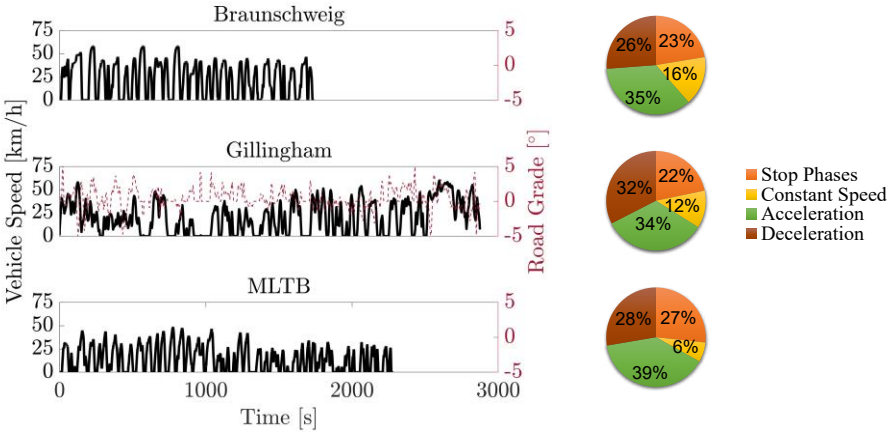

Figure 2. Vehicle speed of the considered driving cycles.

Table 3. Main Features of the considered mission profiles.

	Braunschweig	Gillingham	MLTB
Duration [s]	1740	2875	2281
Distance [km]	10.9	16.6	9.0
Avg. Speed [km/h]	22.5	20.8	14.2
Max Speed [km/h]	58.2	59.9	48.7
Avg. Acc. [m/s²]	0.2	0.2	0.2
Max Acc. [m/s²]	2.4	2.3	1.5
Spec. Energy Demand [kWh/km]	0.90	1.05	0.94

The baseline reference engine is a diesel engine with 3.0L of displacement, downsized to a rated power of 100 kW and modified in order to be exploited for H2 combustion, with a proper benchmark between the cost and the level of complexity [32].Technical specifications of the different components have been set exploiting the outcomes of previous European Commission funded projects such as ZeEUS [33] and on the basis of an extensive literature review and market survey. Concerning the choice of the suitable Electric Motor (EM), at present almost the entire light-duty hybrid vehicle industry has shifted to permanent magnet (PM) machines in order to meet the increasing power density and efficiency requirements [34]. On the contrary, for medium and heavy-duty vehicles induction machines remain an attractive option for their very low drag losses at part load. Nevertheless, the specific market of electrified buses is shifting towards PM electric machines with an average peak nominal power of 200 kW [33]. Finally, a PM synchronous machine has been chosen thanks to its high energy efficiency, delivering a peak power of 200 kW and continuous power of 140 kW. As far as the battery is concerned, at first, the battery sizing and energy content have been fixed, according to the route length and the final desired State of Charge (SOC) [35]. A total installed energy of 20 kWh is considered the most suitable for the present application, with a target maximum power of 200 kW, in consistency with the EM power. Regarding battery chemistry, a high-specific power cell is desirable for a full hybrid series application [36]. In this field, the most exploited chemistries are the ones available with Li-Ion batteries, granting high power densities and life cycles, necessary for long traveled distances [37]. Among the different options, Lithium-ferro-phosphate (LFP) offers a longer life cycle, ensuring lower replacements, with a comparable carbon footprint of battery stack production with respect to other chemistries such as NMC (Lithium Nickel Manganese Cobalt Oxide

 doi:10.20944/preprints202311.1191.v1

battery). In conclusion, the chosen cell is made of LFP, and the main characteristics are reported from [38], with 120 cells in series and 20 in parallel to achieve the target power and density. The main powertrain components' technical specifications are summarized in Table 4.

Table 4. Hybrid powertrain technical specifications.

ICE	**Displacement**	3.0L
	Bore x Stroke	83 x 90 mm
	Features	Single-stage Turbocharger w/ VGT
	Max power	100 kW
EM	**Max power**	200 kW
	Max Torque	1500 Nm
Battery	**Capacity**	19.8 kWh
	Nominal Voltage	396 V
	Maximum Current	2400 A
	Maximum Power	950 kW
	Cell in series	120
	Cell in parallel	20

3. Combustion and fuel injection system

The present section describes the development and optimization of the fuel injection and combustion systems suitable for the H2-fueled internal combustion engine, through both numerical simulation and dedicated experiments in an optically accessible laboratory single-cylinder engine. In particular, the control of the fuel injection and of the combustion process for an hydrogen engine is extremely challenging, due to the high risk of backfire in case of port fuel injection and to the complexity of managing mixture formation through the supersonic flow of the gaseous fuel in case of direct injection. Then, the development of high-fidelity CFD models to enlighten the in-cylinder H2 fuel injection through supersonic flows and to describe accurately the hydrogen combustion, including anomalies such as knock, pre-ignition and misfire, is fundamental to combine high efficiency, low emissions, high specific power output and durability all in one concept.

Injection

Regarding the choice of the fuel injection system, different options have been analyzed, ranging from PFI to DI, as mentioned in Section 2. Indeed, to achieve high power output and efficiency, hydrogen DI is preferable, however, the low hydrogen density leads to supersonic chocked flows, with high penetration and reduced in-cylinder mixing times, despite hydrogen's extremely high laminar diffusivity. Injection pressure levels and nozzle design therefore need to be carefully scrutinized. In this context, high-fidelity Large Eddy Simulations (LES) of the turbulent under-expanded H2 jets can play a crucial role in the fundamental understanding and prediction of the physical mixing process, allowing the design an optimized injector nozzle and associated injection strategies. In addition to high-resolved CFD simulations, also the Reynolds averaged (RANS) modeling approach could be employed as a cost-effective engineering tool to predict and explore several nozzle designs and pressure ratios [39–42] .Boundary and operating conditions are derived from reduced order models (cf. Sections 2 and 5).

As a first step, LES fundamental studies have been conducted on nitrogen jets for validation of the developed injection model, and predictions [39] have been compared with experimental data [42,43] An example is shown in Figure 3, where the contours of the density gradient of the nitrogen jet are presented at different time steps, with 5.8 bar of Nozzle Pressure Ratio (NPR) and 1 bar of ambient pressure, and the predicted axial density is compared for validation against the two reference studies. Normalized centerline density was predicted relatively well, with small phase

Preprints (www.preprints.org) | NOT PEER-REVIEWED | Posted: 20 November 2023 doi:10.20944/preprints202311.1191.v1

difference after the Mach disk, also due to uncertainties in the actual nozzle conical shape [42]. The formation of the barrel-shocks and slip lines, and the rolling up of the initial vortices are well visible.

By increasing the NPR up to 30, and considering actual hydrogen injections, the jet morphology changes substantially, as visible in Figure 4 (left). The higher NPR generates a larger barrel-shock, with only one shock cell. Immediately afterwards, the flow transitions to turbulent flow, which eventually reduces the tip penetration. The expected main characteristics of the jets are captured by the CFD model, such as the turbulent mixing, and the emitted aerodynamic sound. Simulations have also been performed on pintle outward opening nozzles, with similar considerations. Less demanding RANS studies have then been conducted to explore a wide range of injection pressure and back-pressure operating conditions, including the effect of nozzle shape, like inward vs. outward opening (Figure 4,right). In this modeling framework, even if capturing H2 far field mixing remains challenging, RANS results provide an adequate description of the flow physics for engine CFD models allowing the screening of multiple design parameters at an affordable cost.

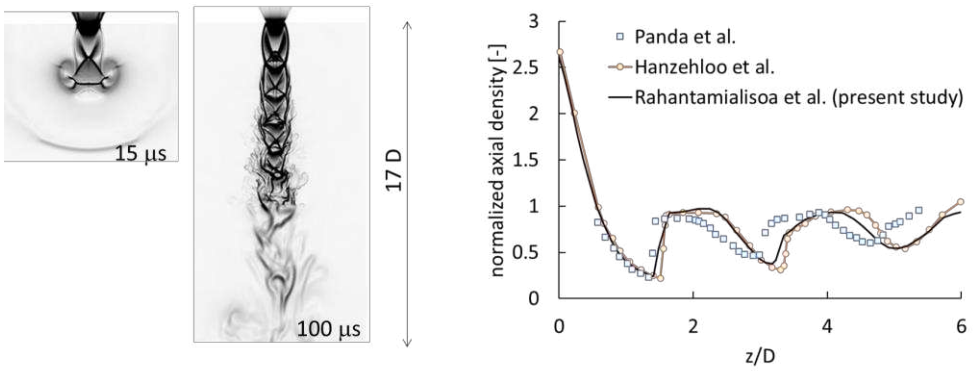

Figure 3. LES of nitrogen injection at 5.8 bar into 1 bar ambient back pressure, through a 1 mm diameter nozzle. Simulation results of the jet development in terms of density gradient over time (left). Normalized axial density vs. axial distance (right), for the present study [39] and two reference studies [42,43].

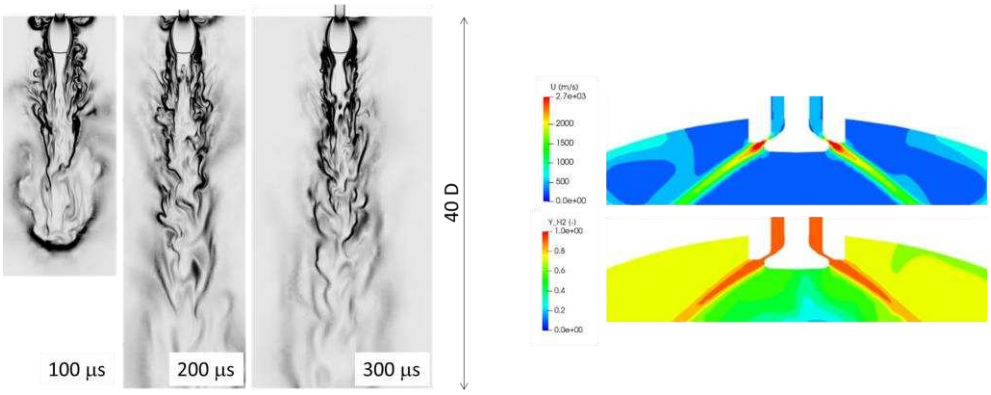

Figure 4. H2 injection simulations at 30 bar into 1 bar. LES simulation of singe hole nozzle; predicted contours of density gradient over time (left) [39]. RANS simulation of a pintle injector; predicted velocity magnitude and fuel mass fraction (right).

Mixture formation

Still today, limited experimental work is available in the literature dealing with H2 jet evolution, mixing and combustion. In order to build a reliable CFD design workflow, quantitative measurements of H2 injection and combustion are needed for validation. Regarding hydrogen mixing in a motored engine, the most comprehensive dataset is available from Sandia's optical hydrogen engine (SOpHy) [44]. Indeed, the CFD modeling capabilities have been tested against

Preprints (www.preprints.org) | NOT PEER-REVIEWED | Posted: 20 November 2023 doi:10.20944/preprints202311.1191.v1

velocity and hydrogen mass-fraction fields measured in these experiments. The considered engine features a central mounter single-hole injector, whose mesh resolution, geometry details, and boundary types were designed based on the previous activity. For the specified motored engine operation [45], various RANS turbulence models within the k- family, grid managements, wall treatments, and turbulent Schmidt numbers have been scrutinized.

The Realizable k- model performed relatively better than others, and its corresponding results are shown in Figure 5 (left) in terms of mixture distribution. In the central column the experimentally measured H2 distribution is presented at two different time steps for the optical accessible window, while in the right column, the simulation results are visible. Comparing the direction and spread of the hydrogen jet, especially at -130 deg., the numerical model can predict correctly the air/gas during the intake stroke, while a slight under-prediction of the mixing is visible at -30 deg. In Figure 5 (right) the results of the turbulent Schmidt number variation are presented on the velocity profile along the cylinder axis. Calibrating the Schmidt number, the hydrogen diffusion predictions are improved to some extent at the end of the compression stroke. Future project analyses regarding the fuel injection system will include the test of other turbulence models, such as Low-Reynolds variants, or Reynolds Stress Model, still within the RANS framework for computationally efficiency.

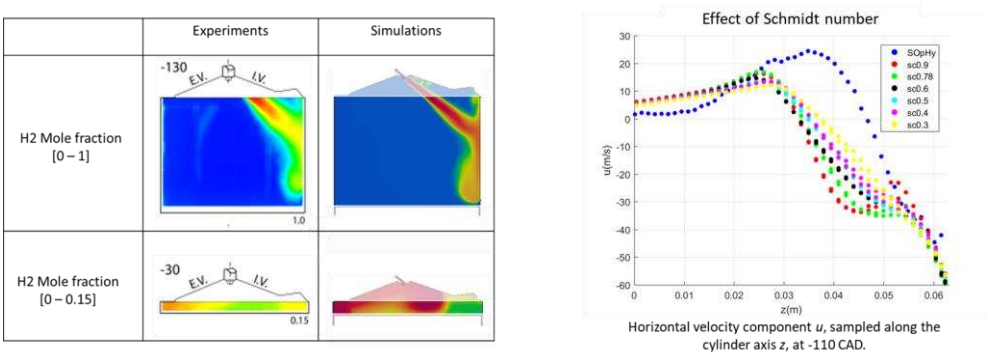

Figure 5. Hydrogen mixing in the motored engine SOpHy [44,45] experiments vs. simulation. Hydrogen mole fraction at two different timings (left), and velocity profile varying the Schmidt number (right).

Full engine model with combustion

In the third step of the analysis, combustion conditions are considered, carrying out a numerical and experimental analysis on the single-cylinder naturally-aspirated optical-access engine of the University of Perugia which allows combustion visualization through the transparent piston and side windows (see Table 5 for more engine details).

Table 5. Optical access engine specifications.

Displacement	500 cc
Bore x Stroke	85 x 88 mm
N. of valves	4
Chamber type	Pent roof

All the results of the combustion experimental measurements will serve as a validation data for both LES and RANS models, to build a reliable and validated CFD model. In particular, various excess air ratios are considered (i.e., $\lambda = 2 \div 3.5$) with two main injection categories:

- premixed cases, meant to reproduce the behavior of a PFI engine assuming that hydrogen and air have perfectly mixed (limiting case);
- DI cases with side-mounted injector and central spark, at various start of injection (SOI).

Preprints (www.preprints.org) | NOT PEER-REVIEWED | Posted: 20 November 2023 doi:10.20944/preprints202311.1191.v1

Simulations were carried out, preliminarily, at 1000 rpm and with 5 bar BMEP. Combustion is modeled using the well-mixed approach, with the LLNL reaction mechanism developed by O'Conaire et al. [46]. Figure 6 presents a comprehensive summary of the combustion numerical analysis, with the mass fraction burned (left, center) at different values of lambda and SOI and the combustion efficiency (right). The port fuel injection cases (black lined) mimicked by premixed assumption show the maximum combustion efficiency at all lambda values (Figure 6, right). Of course, volumetric efficiency will be lower, and a higher intake pressure will be needed to maintain the same load. With DI strategies mixing tends to improve advancing SOI. At λ=3 the fuel mass fraction burned was lower than the premixed case and SOI had no significant effect, while at λ=3.5 SOI had a sensible effect on the fuel mass fraction burned which increases as the SOI is more advanced. The combustion efficiency at λ=3.5 is very poor, and such level of air-fuel ratio cannot be used, at least without further countermeasures.

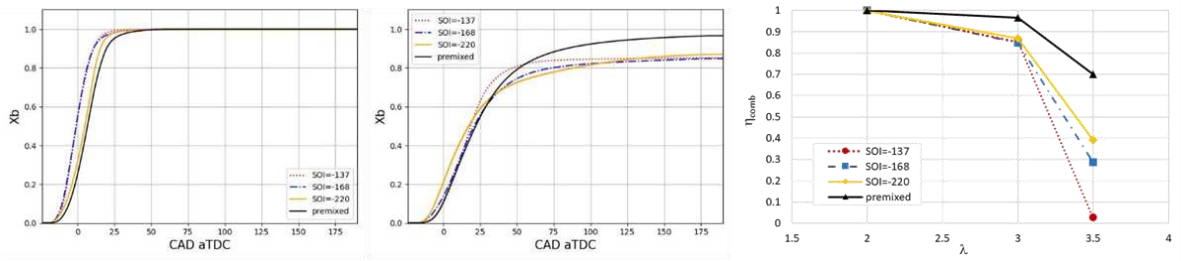

Figure 6. Effect of SOI timing on DI engine combustion at various air excess ratios. Mass fraction burned at λ=2 (left) and λ=3 (center). Combustion efficiency as a function of λ (right).

The main task of this work will then be the metal engine design optimization carried out through thermo-fluid-dynamic simulations of the engine combustion system. RANS simulations can guide injection and combustion systems towards the achievement of targets specified in a previous Section, by tuning injection system design with the piston and chamber geometry design. As a result of the 3D-CFD models, heat release rates can be derived as a function of the combustion system and operating conditions. This data can feed the 1D engine model developed in GT-Power which can be used for the overall engine performance assessment, such as generating engine maps of efficiency, performance and emissions. Based on such calibration and validation step, the 1D engine model will then be used to explore several additional parameters, such as injection strategies, ignition timings, lean stability, Exhaust Gas Recirculation (EGR) rate, boost level, under various speed-load conditions. A crucial aspect will also be the prediction of abnormal combustions, due to pre-ignition and end-gas autoignition, which will rely on calibrated combustion models against preliminary experimental tests on prototype.

4. Waste Heat Recovery technologies and After Treatment System

In parallel with the activities of engine design, the engine subsystems have been developed and optimized, through both experimental and simulation activities. Different WHR technologies have been scrutinized, while for the aftertreatment system, an H2-SCR system has been chosen to achieve near-zero NOx emissions levels, and the analysis is focused on the experimental characterization of the possible catalytic system to be implemented in this device.

WHR technologies

The evaluation of the WHR has been preliminarily assessed on the reference engine: 3.0L turbocharged diesel one. The possibility to test a baseline-like engine mounted on the test bench at the ICE laboratory of the University of L'Aquila gives the availability of engine exhaust data, fundamental to evaluate the energy recovery potential. In particular, the temperature of the exhaust gases T_{exh} is measured after the catalyst and particulate filter devices, in order to preserve their operating conditions. Exhaust mass flow rate m_{exh} is calculated by knowing the engine intake air and

Preprints (www.preprints.org) | NOT PEER-REVIEWED | Posted: 20 November 2023 doi:10.20944/preprints202311.1191.v1

the fuel rate [47]. Figure 7 shows these two quantities and their relations with the engine power. These values are used to estimate the thermal power available for waste heat recovery bottomed sections.

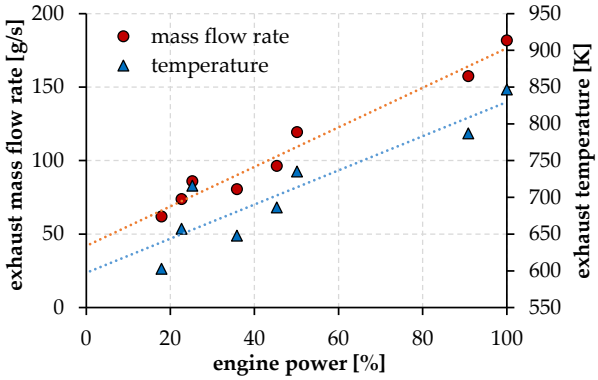

Figure 7. Reference data for engine exhaust mass flow rate and temperature as a function of the engine power, evaluated downstream of the aftertreament devices.

ORC-based unit

The first option studied for WHR is the possibility to introduce an indirect waste heat recovery section, based on an Organic Rankine Cycle (ORC) unit. This is composed by an evaporator, where the energy of the exhaust gases can be exchanged to the organic fluid to vaporize and superheat it, an expander, which converts the thermodynamic energy of the fluid into mechanical and eventually electrical energy, a condenser, which exchange heat towards the cold sink, and a pump to pressurize the fluid and close the thermodynamic cycle (Figure 8). The ORC-based unit proposed has a volumetric machine for expander (of scroll type), suitable for its flexibility and capability to adapt in dynamic and off-design conditions [48,49], and it has been tested specifically to derive a numerical model of the whole ORC unit [50,51]. The model has been validated through experimental data [52] and is based on general assumptions: a) the organic fluid is R245fa; b) the cold sink is cooling water at 45°C, to simulate the cooling condition on board; c) overall amount of fluid is equal to 7 kg; d) pump and expander rotational speeds are controlled to match the thermal power available and to improve the overall performance considering the permeability of the ORC circuit.

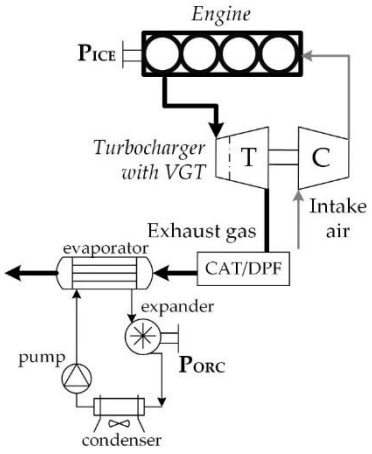

Figure 8. Scheme of the ORC-based unit proposed for exhaust heat recovery.

The control of the pump speed and the contextual one of the expander is needed to have the right mass flow rate of working fluid which matches the most suitable conditions at the evaporator. The evaporating pressure, moreover, is strictly related to the permeability of the circuit, mainly dependent from the WF flow rate and consequently from the entity of the thermal power recovered (i.e., the exhaust gas temperature entering the evaporator). Figure 9 shows the resulted values, which ranges from 10 to 25 bar, almost linearly with the exhaust temperature. It is just the point to notice

Preprints (www.preprints.org) | NOT PEER-REVIEWED | Posted: 20 November 2023 doi:10.20944/preprints202311.1191.v1

that the maximum pressure achieved is not so far from the critical point of the R245fa fluid, and also represents a technical limitation for safety, technology of the components and materials [53].

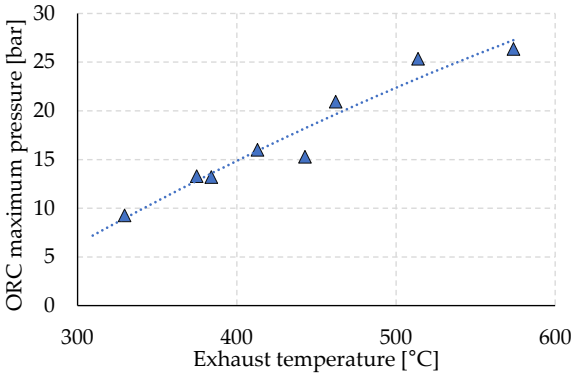

Figure 9. ORC evaporating pressure and exhaust temperature.

The evaporating pressure is also the parameter that sets the ORC efficiency, since the condensing pressure is almost fixed at the value of 4 bar, related to the environmental conditions of the cold sink on board. Figure 10 (left) shows the values of the ORC efficiency, evaluated according to the eq. 1, and ranging from 4 % to 9.5 %, at the maximum pressure:

$$\eta_{ORC} = \frac{P_{ORC}}{P_{exh}} = \frac{P_{expander} - P_{pump}}{m_{exh} c_{p,exh} (T_{exh} - T_{exh,out})} \quad (1)$$

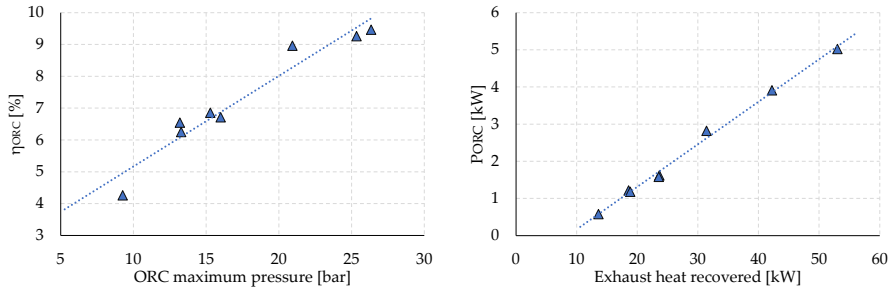

Figure 10. Left: ORC efficiency vs. evaporating pressure; right: ORC net power recovered.

Finally, the net ORC power P_{ORC} is evaluated and plotted vs. the exhaust thermal power recovered from the engine in Figure 10, right. It is up to 5 kW in higher engine power conditions, where the recovered thermal power P_{exh} is equal to 53 kW.

Turbocompound

The second option investigated is a direct recovery, where the same exhaust gases are expanded in an additional turbine, placed downstream of the main turbine of the turbocharger (Figure 11). The possible recovery has been evaluated thanks to a 0D model, where the recovery turbine T_{aux} is represented by a characteristic map (mass flow rate vs. pressure ratio vs. efficiency vs. rotational speed [54]), derived from an existing one and adapted to the specific case study.

Preprints (www.preprints.org) | NOT PEER-REVIEWED | Posted: 20 November 2023 doi:10.20944/preprints202311.1191.v1

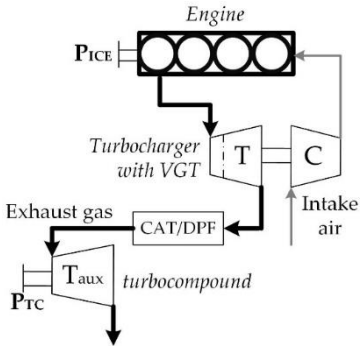

Figure 11. Layout of the turbocompound bottomed to the engine exhaust.

The first result is the pressure ratio of the turbocompound β_{TC}, which is related to the pressure admissible on the exhaust line, since the outlet pressure is close to the environmental one. The increase on turbocompound pressure ratio, so, increase the engine backpressure, although the presence of a variable geometry turbocharger (VGT) mitigates this value on the exhaust manifold of the engine [55,56] and it is considered in the net power estimation ($P_{TC,net}$). Figure 12 shows the turbocompound pressure ratio, which is linearly dependent on the exhaust temperature T_{exh} (i.e. turbocompound inlet temperature) and ranges from 1.2 to 1.6. For engine exhaust temperatures lower than 350°C, the available thermal power is not sufficient to drive the turbocompound, and the resulting pressure ratio is too low.

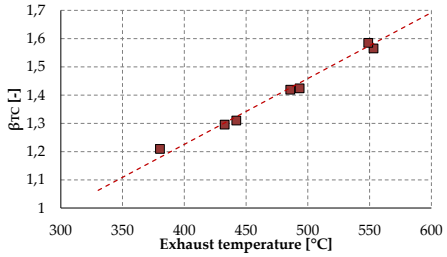

Figure 12. Turbocompound pressure ratio and exhaust temperature (i.e. turbocompound inlet temperature).

The operating of the turbocompound is evaluated thanks to a characteristic map of the additional turbine, where the efficiency η_{TC} is a function of the specific working point in terms of mass flow rate and pressure ratio. In Figure 13 (left), the efficiency is plotted in relation to the exhaust mass flow rate m_{exh}: the values are ranging from 55% to 68%, and this opens for a possible optimization of the design of the machine for the specific application.

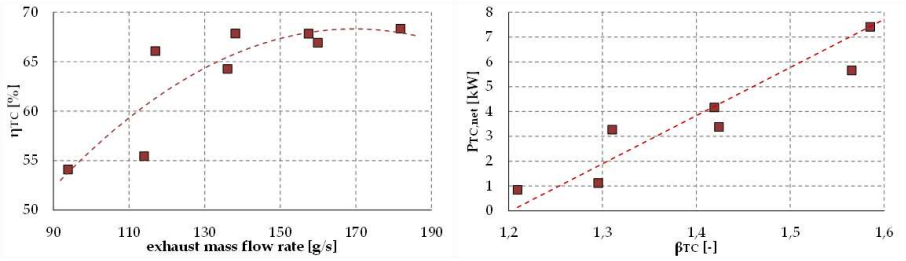

Figure 13. Left: Turbocompound efficiency vs. exhaust mass flow rate crossing the auxiliary turbine. Right: Final net power recovered by the turbocompound vs. pressure ratio of the turbine.

Finally, the net turbocompound power has been reported in Figure 13 (right). The values are up to 8 kW and linearly dependent on the pressure ratio across the auxiliary turbine. As already stated, this dependence is limited by the backpressure effect on engine: if the pressure ratio on the turbine is

 doi:10.20944/preprints202311.1191.v1

higher, the side effect on the engine can overcome the increase of turbocompound power and nullify the recovery.

Engine side effects

The introduction of the WHR section on the exhaust gases line will produce an unavoidable engine backpressure increase. This could be more significant for turbocompound specifically if it is placed downstream the turbocharger (series turbocompound). However, also if a parallel turbocompound is considered, the rearrangement of the equilibrium of the turbocharger, to meet the request of the boost pressure and leave room for possible recovery, could produce a backpressure increase in the exhaust manifold. In this case, the possibility of introducing two sections of waste heat recovery, combining direct and indirect ways can significantly increase the recovery and better exploit the available thermal energy from the exhausts [57]

Considering ORC-based unit, the backpressure increase is strongly related to the permeability of the heat exchanger used as an evaporator, on the gas side. In this case, the technology chosen for this component is crucial. Finned tube heat exchangers seem to have the best performances in this regard [58] and, if these pressure drops are limited (e.g. < 100 mbar), the negative effect of the engine can be neglected. However, the introduction of ORC-unit is more invasive than the turbocompound and requires more space on board. Moreover, it introduces a non-negligible extra-weight, whose influence on the propulsive power should be estimated. But, considering the application of the H2-ICE project (i.e. 12 m bus), this extra-weight could not be so significant if related to the overall weight of the vehicle and its payload.

SCR system

Although the H2- fueled engine is intended to operate with extreme lean mixture, thus producing low NOx emissions, the target of the hybrid-bus application is to reach almost zero emissions. Therefore, NO_x abatement by after-treatment system is still mandatory and is at present based on SCR [59]. Currently, the SCR system is based on a technology that consists of reductive treatment with ammonia (NH_3-SCR) to catalytically convert NO_x into nitrogen (N_2) and water (H_2O) molecules. Due to the toxicity and hazardous nature of ammonia, it is produced in vehicles using an aqueous solution, called AdBlue, containing 32.5 wt.% urea $CO(NH_2)_2$ [60]. This additive is stored in a separate tank and injected before the SCR converter into the gas stream leaving the particulate filter, where the urea thermally decomposes to produce isocyanic acid (HNCO) and ammonia (NH_3) [61]. Although ammonia and urea are currently the preferred choice for the selective catalytic reduction of NOx, hydrogen has recently attracted strong interest as a reducing agent, representing a rather interesting alternative. Indeed, in recent years, several researchers have focused their studies on the development of a suitable catalytic system for the selective catalytic reduction of NOx using hydrogen (H_2-SCR [62–64]). The latter technology has several advantages: zero carbon footprint, as there is no formation of CO and CO_2 molecules during NO_x removal; formation of water from hydrogen combustion (O_2 present in the gas stream); high NO_x conversion activity at lower temperatures (T<200°C) with respect to NH_3-SCR counterparts (T=350-400°C) [65]; possibility of drawing from a single tank using hydrogen also as a fuel to partially replace diesel or petrol in the combustion mixture. There are four main reactions that occur in selective catalytic reduction with hydrogen in the presence of oxygen, but the desiderated one has two NO molecules reacting with four hydrogen molecules to form N_2 [59,62]. Studies reported so far in the literature have shown a low selectivity towards N_2 production with undesirable productions of partially reduced species such as N_2O and NH_3.

As a first step, the preparation of suitable catalytic systems using palladium (Pd) as the active phase and metal oxides as supports is the object of the study. These catalytic systems could be deposited on monolithic cordierite support [66], for the realization of a system that can be implemented in the last stage of treatment in diesel engine flue gas purification. In particular, the catalytic support that is to be developed consists of the mixture of the two metal oxides CeO_2 and ZrO_2 and of a Pd-based active catalytic phase (hereinafter called PCZ). Figure 14 shows the diffraction

Preprints (www.preprints.org) | NOT PEER-REVIEWED | Posted: 20 November 2023 doi:10.20944/preprints202311.1191.v1

patterns of the raw CeO_2 (a) and ZrO_2 (b) powders, of the mixture CeO_2-ZrO_2 (c), and the complete catalytic system (active phase and catalytic support) Pd/CeO_2-ZrO_2 (d). The CeO_2-ZrO_2 catalytic support (c) shows peaks attributable to the crystalline phases of the starting metal oxides and the Pd/CeO_2-ZrO_2 (PCZ) catalytic system (d) shows a diffraction pattern with narrower peaks than the only support. The crystalline phases of Pd cannot be appreciated, due to the small quantity of metal on the catalytic support.

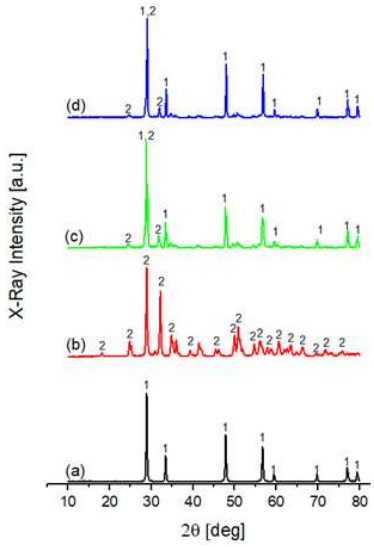

Figure 14. X-ray diffraction pattern of CeO2 (a) and ZrO2 (b) precursor powders, CeO2-ZrO2 catalytic support (c) and catalytic system Pd/CeO2-ZrO2 (d); 1=Cerianite, CeO2; 2=Zirconium Oxide, ZrO2.

Figure 15 shows micrographs at various magnifications of the PCZ catalytic system. From these micrographs, it is possible to see a very regular and compact surface in which there is good interaction between the two metal oxides that act as the catalytic support. Specifically, one can observe areas (circled in red) with a regular spherical morphology attributable to cerium oxide and areas (circled in green) with a smaller average crystalline domain size attributable to zirconium oxide. The structure of the produced support material thus presents the two support oxides evenly distributed in space with exposed sites of both precursors.

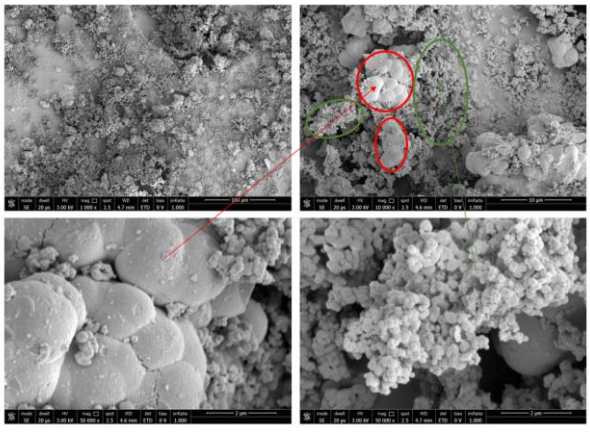

Figure 15. SEM micrographs at various magnifications of the Pd/CeO2-ZrO2 catalytic system.

As a second step, small scale prototypes of coated cordierite substrate will be tested with real currents emitted by a diesel engine at the test bed, studying the degree of conversion and selectivity of the catalyst under different engine operating conditions and with different flow rates of H_2. The experimental setup is schematized in Figure 16. The reagent mixture is obtained by flowing the

Preprints (www.preprints.org) | NOT PEER-REVIEWED | Posted: 20 November 2023 doi:10.20944/preprints202311.1191.v1

exhaust gases downstream of the turbine. The hydrogen is injected on the prototype exhaust gas line upstream of the H2-SCR reactor.

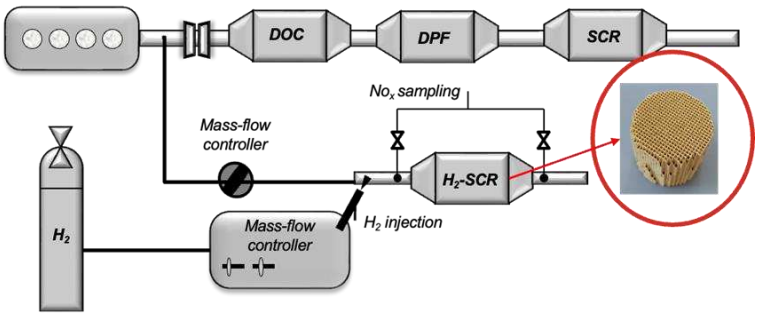

Figure 16. Experimental setup scheme for the small scale substrate prototype.

5. Engine and Hybrid Powertrain management

The present section describes the development of the engine and hybrid power-train management strategies. On the one hand, the load control of H2-ICEs is crucial to ensure good performance and low emissions: a proper control strategy is required to avoid the risk of combustion anomalies (e.g., knock and preignition) while limiting NOx emissions and enhancing engine efficiency. As a starting point, a set of data has been generated from the 1D engine model calibrated in GT Power. A fast running engine model based on Artificial Neural Networks (ANN) has then been developed, based on GT Power results. The advantage of such model is the low computational time, which makes it suitable for the development of the H2-ICE control strategy using a Model-In-the-Loop (MIL) approach. On the other hand, since in a hybrid powertrain both fuel economy and pollutants emissions reduction strongly depend on the exploitation of each energy source (i.e. fuel and battery), a supervisory high level control strategy is mandatory to determine the power which has to be delivered by each source. Two optimization methodologies will behave been developed for the design of the energy management strategies, the former one based on a heuristic Dynamic Programming (DP) Rule-Based approach, the latter based on the application of Pontryagin's Minimum Principle (PMP) for the minimization of the equivalent fuel consumption (ECMS). Both approaches are intrinsically causal as they do not request requiring the a-priori knowledge of the mission profile, nevertheless this information is accounted for in the design process to improve the accuracy of the strategy in reaching a target SOC. It is worth noting that. Although for urban buses, for which the route is defined a priori, this could be a non-critical issue., the high computational demand makes DP not suitable for real-time application. Therefore, the DP solution will be assumed as a benchmark for an assigned route, while, in order to overcome the issues of both high computational demand and a-priori knowledge of mission profile, a further energy management strategy will be designed based on the Pontryagin's Minimum Principle (PMP).

Engine Model Description

The engine model has been developed in Matlab/Simulink starting from available data of the H2-ICE. To cover as much as possible the whole operating envelope, the engine model has been validated in a wide operational range for each of the controllable variables as shown in Table 6.

Table 6. Engine Model Limits.

Variable	Range
Speed [rpm]	[1000 - 4000]
BMEP [bar]	[2 – max BMEP available for given RPM]
CA50 [deg]	[-30 - 30]
Lambda [-]	[2 – 2.7]
EGR [%]	[0 – 10]

Preprints (www.preprints.org) | NOT PEER-REVIEWED | Posted: 20 November 2023 doi:10.20944/preprints202311.1191.v1

The engine model is necessarily coupled to the control strategy: indeed, the inputs of the model are the outputs of the control strategy, thus all the modelled quantities have to be directly or indirectly (e.g., derived from an intermediate block) calculated based on the control actions: this makes the simulation a loop including the engine model and the engine controller. The model outputs concern combustion metrics, intake and exhaust conditions, as shown in the I/O sketch reported in Figure 17.

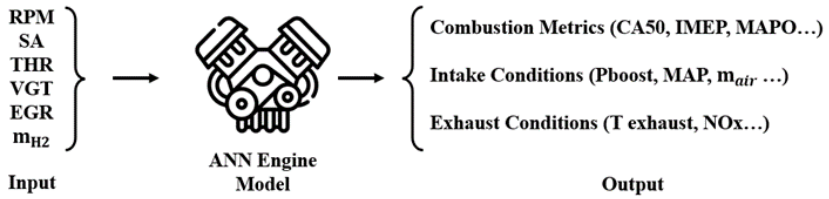

Figure 17. Input and output of the engine model.

The modelling approach allows representing the cycle-by-cycle behaviour: it can be explained taking as example the generation of Indicated Mean Effective Pressure (IMEP) as shown in Figure 18:

1. The intake conditions, in terms of air mass and EGR percentage are estimated from the intake block;
2. RPM, Spark Advance (SA), mass of fuel and the intake conditions are the input parameters for the Crank Angle of 50% heat release (CA50) ANN;
3. CA50, intake conditions, mass of fuel, RPM and VGT position are the input for the IMEP ANN.

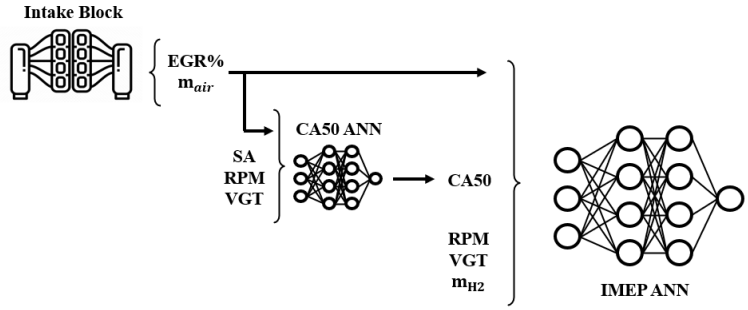

Figure 18. Input and output of the engine model, IMEP example.

Table 7 summarizes the accuracy of the engine model (compared to reference data) in steady state conditions, in terms of Root Mean Square Error (RMSE) and percentual RMSE.

Table 7. Engine Model Accuracy.

Variable	RMSE	RMSE %
CA50 [deg]	0.34	0.56
IMEP [bar]	0.033	0.33
BSFC [g/kWh]	2.26	0.75
Pcyl, max [bar]	0.51	0.43
Tcyl, max [K]	6.57	0.41
NOx (below 2000 ppm) [ppm]	11	0.56
P Exhaust [bar]	0	0.3
T Exhaust [K]	2.3	0.57

As shown in Table 7, the percentage RMSE is always lower than 1% for each predicted variable. Once the model has been validated in steady state conditions, the capability of representing cycle by cycle variations has been introduced. Specifically, two additional ANNs have been introduced, to

Preprints (www.preprints.org) | NOT PEER-REVIEWED | Posted: 20 November 2023 doi:10.20944/preprints202311.1191.v1

properly represent the statistical distribution of CA50, which propagates to other combustion metrics. For knock intensity, a further statistical dispersion is used to represent Maximum Amplitude Pressure Oscillation (MAPO) variations at fixed CA50 levels. Finally, the model has been completed with intake manifold and turbocharger dynamics. Figure 19 shows a comparison, in terms of BMEP, Brake Specific Fuel Consumption (BSFC) and NOx, between the GT Power and the Simulink model outputs in a transient simulation where RPM, VGT, Throttle Valve (THR), SA and mass of injected fuel change. As it is possible to see, the model is capable to replicate the engine behaviour in terms of torque production, consumption and emissions.

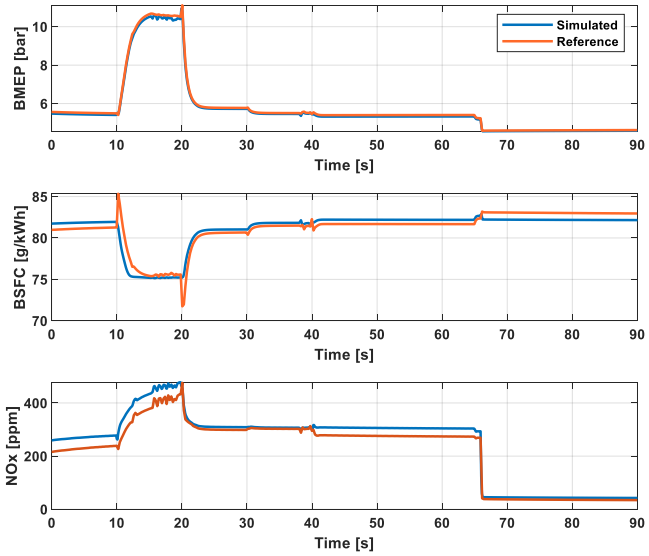

Figure 19. BMEP, BSFC and NOx simulated in GT Power during a transient and BMEP simulated from the presented engine model.

Control Strategy Description

Once the engine model has been validated, a torque control strategy has been implemented. The inputs of the latter are the requested BMEP at the current RPM, the manifold and boost pressure and the feedback from a combustion analyser (CA50, Pcyl, max and MAPO), as shown in Figure 20. Based on these inputs, the control strategy set the position of the actuators (e.g., SA, THR, VGT…).

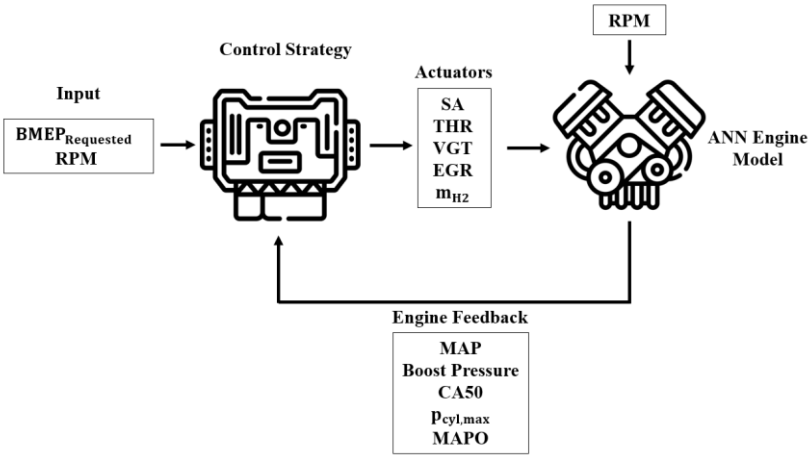

Figure 20. Input and output of the control strategy.

In order to avoid abnormal combustions (e.g., knock, preignition…) and limit NOx emissions, the lambda value has to be above 2.2, thus the load control can be directly managed with the amount

Preprints (www.preprints.org) | NOT PEER-REVIEWED | Posted: 20 November 2023 doi:10.20944/preprints202311.1191.v1

of injected fuel. However, the fuel request has to be saturated between the knock and misfire conditions in order to keep the engine in safe operating conditions. As regards combustion phasing, a proper control on CA50 position results crucial in order to maximize efficiency without compromising reliability. For this purpose, a CA50-based control strategy has been implemented. The target CA50 is defined as a function of the current operating condition (RPM, load request, EGR and lambda) and saturated under knocking conditions. The SA allowing to achieve the target CA50 for the current conditions is then calculated by means of a dedicated ANN. Moreover, the open loop positions of the THR, VGT and EGR settings are calculated from calibrated maps as function of engine speed and load request. Finally, a closed loop control has been developed, on manifold pressure and boost pressure, acting respectively on THR and VGT. Figure 21 shows an example of the control strategy behaviour. As it can be noticed, the engine is capable to follow the BMEP request also under transient conditions.

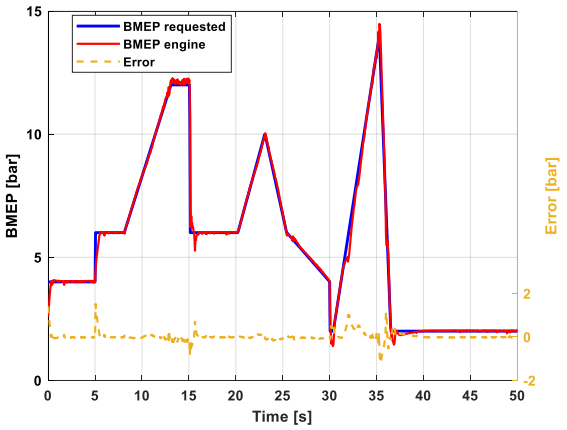

Figure 21. BMEP request, BMEP provided and error.

Figure 22 shows the actuators (THR, VGT, SA, fuel) settings and the corresponding achieved CA50. It is worth noticing how after a sudden drop in the requested BMEP, the control strategy saturates the minimum requestable fuel and retards the CA50 to keep the BMEP at target.

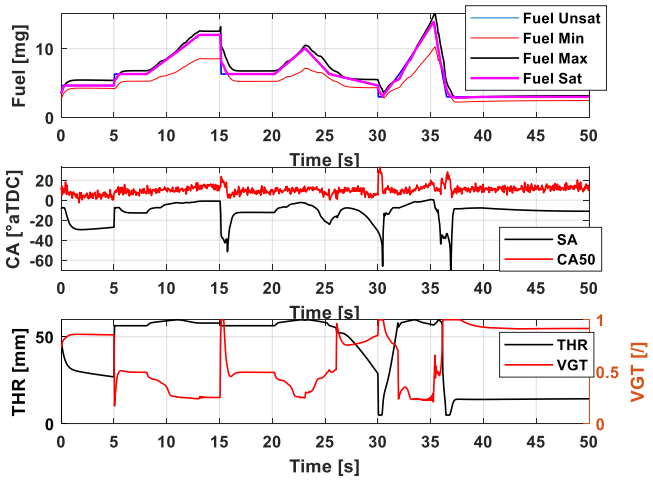

Figure 22. Fuel, SA, CA50, THR and VGT over time.

Hybrid powertrain management

The data flow used to create the vehicle model are shown in Figure 23. Starting from fitting the experimental data of the various vehicle components and vehicle parameters, the optimal operating points of the Range Extender (i.e., ICE+EG) were identified as a function of speed and torque through

Preprints (www.preprints.org) | NOT PEER-REVIEWED | Posted: 20 November 2023 doi:10.20944/preprints202311.1191.v1

an optimization process. This is made possible by the series architecture of the Powertrain, which allows its fixed-point operation.

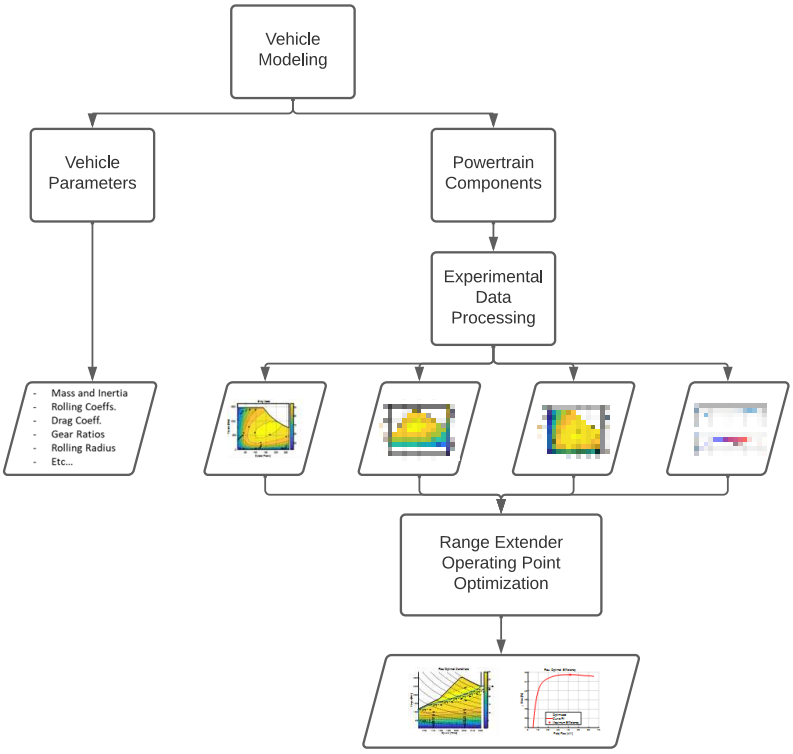

Figure 23. Vehicle Modeling Data Flow.

Two energy management strategies (EMS) have been developed. Specifically, a causal rule-based strategy and a non-causal strategy that uses an optimization process based on the Pontryagin minimum principle (PMP). The rule-based strategy has been implemented to achieve a causal non-optimal benchmark to be used as a reference for tuning the optimized PMP strategy.

Rule Based Strategy

The EMS consists of a Rule Based (RB) controller of the ICE-EG, in which the state variable is the battery SoC [16], as can be seen in Equation (2):

$$\begin{Bmatrix} \xi_{target} = \xi_{start} + \frac{\xi_{end} - \xi_{start}}{distance} * \int vdt = \xi_{start} + \xi_{rate} * \int vdt \\ \xi_{Max} = \xi_{target} * toleranceMax \\ \xi_{Min} = \xi_{target} * toleranceMin \\ \xi_{HardMin} = \xi_{target} * toleranceHardMin \end{Bmatrix} \quad (2)$$

The ICE-EG is switched on when the SoC reaches the lower threshold ξ_{Min}, and is switched off when the SoC reaches the upper threshold ξ_{Max}. The upper and lower thresholds are time-dependent and are calculated as a function of the target SoC (ξ_{target}), which exhibits a decreasing trend along the driving transient, in accordance with the expected battery discharge rate.

An additional activation threshold for the ICE-EG ($\xi_{HardMin}$) is also provided, in which, in the event of excessive battery discharge, more power is requested to cope with an unexpected increase in load. The flow chart of the rule-based EMS is shown in Figure 24.

Preprints (www.preprints.org) | NOT PEER-REVIEWED | Posted: 20 November 2023 doi:10.20944/preprints202311.1191.v1

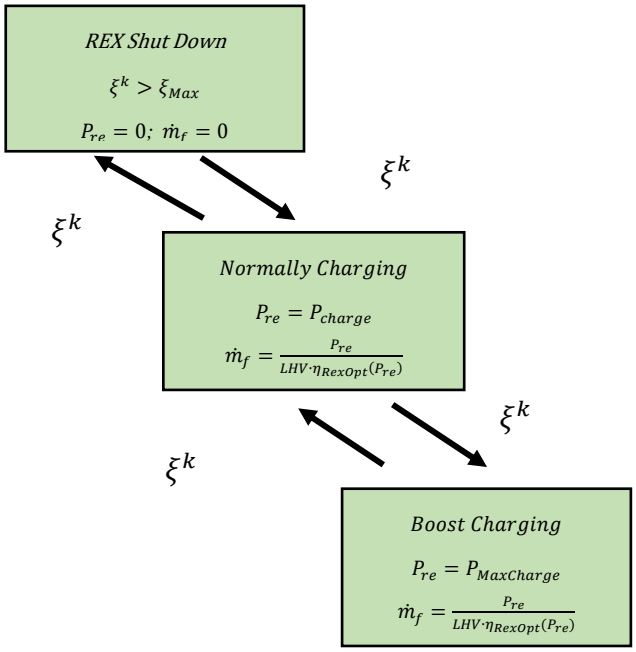

Figure 24. Rule Based Flow Chart.

Figure 25 shows the time trajectory of the battery state-of-charge with the different SOC thresholds for a generic driving cycle.

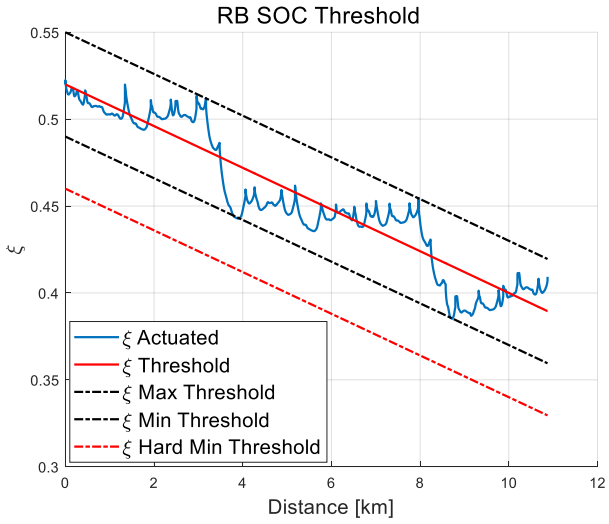

Figure 25. SoC Thresholds.

Pontryagin minimum principle

The Pontryagin Minimum Principle (PMP) is a crucial tool in the study of optimal control problems for dynamic systems. It addresses the challenge of finding the best trajectory that minimizes a given performance criterion, subject to the system's dynamics and constraints. Further theoretical details on the principle could be found in [67], while examples of its application to the HEV powertrain control can be found, e.g., in [68,69]

In the current application, the problem is formulated by considering the battery state of charge (SOC) as state variable and the battery power (P_b) as control variable. The Hamiltonian can be defined as the sum of the fuel mass consumed by the engine and an equivalent fuel mass consumed by the electric motor weighted by an equivalence factor, represented by the co-state (l), thus leading to an Equivalent Consumption Minimization Strategy (ECMS). The co-state drives the solution alternatively towards battery charging or battery depleting and the ECMS-based technique

Preprints (www.preprints.org) | NOT PEER-REVIEWED | Posted: 20 November 2023 doi:10.20944/preprints202311.1191.v1

minimizes the Hamiltonian while adjusting the equivalent factor dynamically over time in order to guarantee the charge stustaining along the whole reference driving cycle. Figure 26 shows the results of the co-state identification and the deviation of the final SOC vs. the target value corresponding to the initial one.

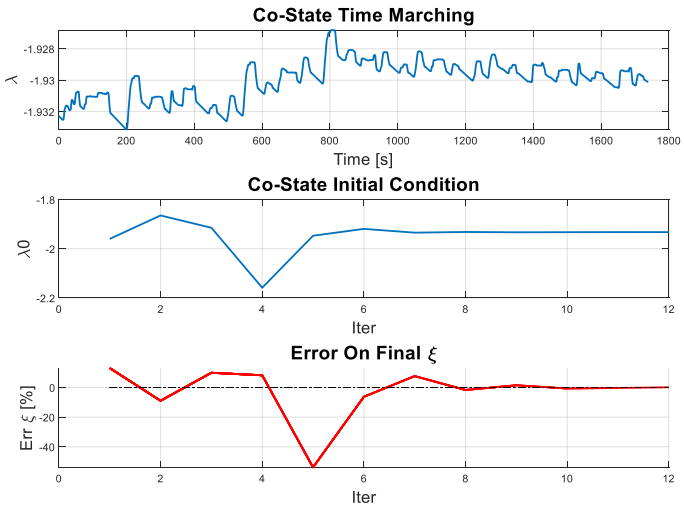

Figure 26. Co-State Identification results.

Table 8 compare the results in terms of fuel consumption and powertrain efficiency achieved by the two proposed EMS (i.e., Rule Based and PMP) for the three driving cycles considered. It can be noted that the use of the optimization strategy leads to an improvement (on average, 9%) compared to the use of the causal strategy. It is worth noting that the fuel consumption is still higher than the imposed target of 10 kg/100 km, nevertheless a significant reduction is expected to be achieved by further improvements of engine combustion system and control, implementation of WHR technologies and further refinement of EMS. Figure 27 shows the time trajectories of SOC and cumulative fuel consumption, evidencing that both RB and PMP guarantee suitable charge sustaining along the whole driving cycles though the former EMS exhibits larger SOC deviation from the mean value, especially in Braunschweig and MLTB cycle.

Table 8. Simulations results: PMP vs RB.

Simulation Results						
Road cycle	Braunschweig		Gillingham Uphill		MLTB	
EMS	PMP	RB	PMP	RB	PMP	RB
Fuel consumption [kg/100km]	11.578	12.694	13.604	14.882	14.803	16.342
D [%]	-8.789		-8.586		-9.415	
$\bar{\eta}_{powertrain}$ **[%]**	24.208	22.039	25.915	23.715	26.259	23.766

where the powertrain efficiency, $\bar{\eta}_{powertrain}$, is defined as in eq. 3:

$$\bar{\eta}_{powertrain} = \frac{E_{wheels}+E_{Aux}}{E_{Rex}+E_{battery}} \quad (3)$$

Preprints (www.preprints.org) | NOT PEER-REVIEWED | Posted: 20 November 2023 doi:10.20944/preprints202311.1191.v1

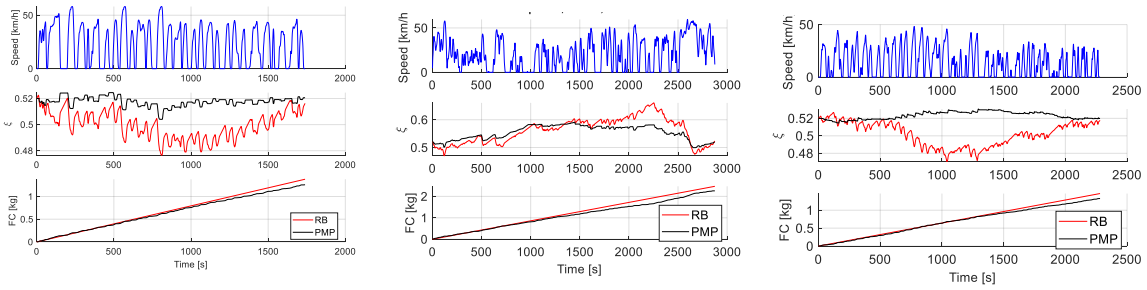

Figure 27. Fuel consumption and state of charge time trajectories achieved by RB and PMP for the three driving cycles. Braunschweig (left), Gillingham (center), MLTB (right).

6. Conclusions and future steps

In the present work, preliminary results achieved to date from the H2-ICE project were presented. A comprehensive methodology has been developed to support the design of engine concepts and vehicle sub-systems for the efficient exploitation of H2 as a fuel, as well as for their integration in a hybrid powertrain for an urban bus application. High fidelity CFD models have been developed and validated to assess the potential of different injection options from Port Fuel Injection (PFI) to Direct Injection (DI), with different levels of nozzle designs and pressure ratios, and to control and optimize the combustion, setting a maximum of $l = 3$ to keep the combustion efficiency above the 85%. Two different Waste Heat Recovery (WHR) systems have been analyzed and tested, to enhance engine efficiency at higher levels: for a direct heat recovery system based on the Organic Rankine Cycle (ORC) a net recovered power of 5 kW has been obtained in higher engine power conditions, while for an indirect turbocompound it is up to 8 kW recovered power, limited by engine backpressure effects. Regarding the aftertreatment system, the preparation of suitable catalytic systems for the Selective Catalytic Reduction (SCR) of NOx using hydrogen as a reducing agent has been completed. Moreover, a dedicated control strategy has been developed exploiting a fast-running engine model based on Artificial Neural Networks (ANN) together with the torque control strategy. Finally, two approaches of Energy Management System (EMS) have been tested to target the desired fuel consumption (i.e., 0.1 kg/km) and to guarantee a suitable SCR operation: a Rule Based (RB) approach and a strategy base on the Pontryagin Minimum Principle (PMP). A gain on the fuel consumption near 10% is obtained with the PMP strategy, with respect to the RB one, on the different considered driving cycles.

Future steps of the project will be focused on:

- further developing the engine combustion system, also exploiting the outcomes of the upcoming experimental campaign on the mentioned single-cylinder optical-access engine,
- assessing the capability of the two WHR systems tested for different operating conditions, and consider the possibility of introducing two sections of WHR, combining direct and indirect ways to increase the recovery,
- giving additional insights on the behavior of the H2-SCR reactor with the experimental testing of small-scale prototypes on a wide range of operating conditions,
- optimizing the Energy Management System (EMS) to reach the desired target in terms of fuel consumption over the different mission profiles.

Then, the final outcome of the project would be not only the development of a traction system for a new generation of H2-ICE but also the enhancement of the know-how for sustainable H2 exploitation in the context of public transport mobility.

Author Contributions: Conceptualization, I.A., M.B., R.C., E.C., F.M; methodology, P.P.B., D.D., B.P.P., L.R., J.Z.; validation, P.P.B., D.D., A.O., L.R., J.Z., formal analysis, I.A., M.B., R.C., E.C., F.M.; investigation, P.P.B., A.O., L.R., J.Z. ; writing—original draft preparation, I.A., M.B., P.P.B., D.D., B.P.P.; writing—review and editing, I.A., M.B., R.C., E.C., F.M., L.R.; supervision, I.A., M.B., R.C., E.C., F.M.; project administration, I.A., M.B., R.C., E.C., F.M.; funding acquisition, I.A., M.B., R.C., E.C., F.M. All authors have read and agreed to the published version of the manuscript.

 doi:10.20944/preprints202311.1191.v1

Funding: Research funded by MIUR - Ministero dell'Istruzione, dell'Università e della Ricerca (2020R92Y3Z).

Data Availability Statement: The data presented in this study are partially available on request from the corresponding author.

Conflicts of Interest: The authors declare no conflict of interest.

Abbreviations

ANN	Artificial Neural Networks
BEV	Battery Electric Vehicle
BMEP	Break Mean Effective Pressure
BSFC	Brake Specific Fuel Consumption
CA50	Crank Angle of 50% heat release
CFD	Computational Fluid Dynamics
DI	Direct Injection
DP	Dynamic Programming
EGR	Exhaust Gas Recirculation
EM	Electric Motor
EMS	Energy Management System
EU	European Union
FCEV	Fuel Cell Electric Vehicle
GHG	Green House Gases
HDV	Heavy Duty Vehicle
ICE	Internal Combustion Engine
IMEP	Indicated Mean Effective Pressure
IVO	Intake Valve Opening
LDV	Light Duty Vehicle
LES	Large Eddy Simulation
LFP	Lithium-Ferro-Phosphate
MAPO	Maximum Amplitude of Pressure Oscillations
MIL	Model-In-the-Loop
NMC	Lithium Nickel Manganese Cobalt Oxide battery
NPR	Nozzle Pressure Ratio
ORC	Organic Rankine Cycle
Pcyl, max	Maximum in-cylinder Pressure
PFI	Port Fuel Injection
PM	Permanent Magnet
PMP	Pontryagin Minimum Principle
RANS	Reynolds-Averaged Navier–Stokes
RB	Rule Based
RMSE	Root Mean Square Error
RPM	Revolution Per Minute
SA	Spark Advance
SCR	Selective Catalytic Reduction
SOC	State Of Charge
SOI	Start Of Injection
SOpHy	Sandia's Optical Hydrogen engine
Tcyl, max	Maximum in-cylinder Temperature
THR	Throttle Valve
V2X	Vehicle To Everything
VGT	Variable Geometry Turbocharger

WF	Working Fluid
WHR	Waste Heat Recovery

References

1. UNECE, European green deal: commission proposes transformation of eu economy and society to meet climate ambitions. https://ec.europa.eu/commission/presscorner/detail/en/IP_21_3541, 2021.
2. IEA, Largest end uses of energy by sector in selected iea countries. https://www.iea.org/data-and-statistics/charts/largest-end-uses-of-energy-by-sector-in-selected-iea-countries-2019, Jul. 2023.
3. EEA, Greenhouse gas emissions from transport in europe. https://www.eea.europa.eu/ims/ greenhouse-gas-emissions-from-transport, Jul. 2023.
4. ACEA, Fact sheet: CO2 standards for heavy-duty vehicles. https://www.acea.auto/fact/ fact-sheet-co2-standards-for-heavy-duty-vehicles/, Jul. 2023.
5. E. Commission, Proposal for a regulation of the european parliament and of the council amending regulation (eu) 2019/1242 as regards strengthening the co2 emission performance standards for new heavyduty vehicles and integrating reporting obligations, and repealing regulation (eu) 2018/956, Jul. 2023.
6. Zhang, C., Zhao, X., Sacchi, R., and You, F., "Trade-off between critical metal requirement and transportation decarbonization in automotive electrification," *Nat Commun* 14(1), 2023. https://doi.org/10.1038/s41467-023-37373-4.
7. Mareev, I., Becker, J., and Sauer, D.U., "Battery dimensioning and life cycle costs analysis for a heavy-duty truck considering the requirements of long-haul transportation," *Energies* 11(1), 2018. https://doi.org/10.3390/en11010055.
8. Çabukoglu, E., Georges, G., Küng, L., Pareschi, G., and Boulouchos, K., "Battery electric propulsion: an option for heavy-duty vehicles? Results from a Swiss case-study," *Transp Res Part C Emerg Technol* 88:107–123, 2018. https://doi.org/10.1016/j.trc.2018.01.013.
9. Moriarty, P. and Honnery, D., "Prospects for hydrogen as a transport fuel," *Int J Hydrogen Energy* 44(31):16029–16037, 2019. https://doi.org/10.1016/j.ijhydene.2019.04.278.
10. Sharma, S. and Ghoshal, S.K., "Hydrogen the future transportation fuel: From production to applications," *Renewable and Sustainable Energy Reviews* 43:1151–1158, 2015. https://doi.org/10.1016/j.rser.2014.11.093.
11. Kim, H., Hartmann, N., Zeller, M., Luise, R., and Soylu, T., "Comparative tco analysis of battery electric and hydrogen fuel cell buses for public transport system in small to midsize cities," *Energies (Basel)* 14(14), 2021. https://doi.org/10.3390/en14144384.
12. Vodovozov, V., Raud, Z., and Petlenkov, E., "Review of Energy Challenges and Horizons of Hydrogen City" Buses, *Energies* 15(19), 2022. https://doi.org/10.3390/en15196945.
13. Heid, B., Martens, C., and Orthofer, A., "How hydrogen combustion engines can contribute to zero emissions," *McKinsey & Company*, 2021.
14. Verhelst, S., "Recent progress in the use of hydrogen as a fuel for internal combustion engines," *Int J Hydrogen Energy* 39(2):1071–1085, 2014. https://doi.org/10.1016/j.ijhydene.2013.10.102.
15. Verhelst, S. and Wallner, T., "Hydrogen-fueled internal combustion engines," *Progress in Energy and Combustion Science, 35*, 490–527, 2009. https://doi.org/10.1016/j.pecs.2009.08.001.
16. HyFLEET:CUTE, Hydrogen Transport, Bus Technology & Fuel for today and for a Sustainable Future. , Jul. 2023.
17. SunLine Transit Agency Hydrogen-Powered Transit Buses: Third Evaluation Report. https://www.nrel.gov/docs/fy08osti/43741-1.pdf, Jul. 2023.
18. Matthias, N.S., Wallner, T., and Scarcelli, R., "A Hydrogen Direct Injection Engine Concept that Exceeds U.S. DOE Light-Duty Efficiency Targets," *SAE Int J Engines* 5(2):838–849, 2012. https://doi.org/10.4271/2012-01-0653.
19. Koch, D.T., Sousa, A., and Bertram, D., "H2-Engine Operation with EGR Achieving High Power and High Efficiency Emission-Free Combustion," 2019.
20. Golisano, R., Scalabrini, S., Arpaia, A., Pesce, F., Vassallo, A., Borgia, F., Cubito, C., Biasin, V., Knichel, T., Millo, F., Rolando, L, Piano, A., "Hydrogen Internal Combustion Engine & KERS: an Appealing Value-Proposition for Green Power Pack," *42nd International Vienna Motor Symposium*, 2021.
21. Millo, F., Rolando, L., Fuso, R., and Zhao, J., "Development of a new hybrid bus for urban public transportation," *Appl Energy* 157:583–594, 2015. https://doi.org/10.1016/j.apenergy.2015.03.131.

22. Wang, L., Yang, Z., Huang, Y., Liu, D., Duan, J., Guo, S., and Qin, Z., "The effect of hydrogen injection parameters on the quality of hydrogen–air mixture formation for a PFI hydrogen internal combustion engine," *Int J Hydrogen Energy* 42(37):23832–23845, 2017. https://doi.org/10.1016/j.ijhydene.2017.04.086.
23. Li, Y., Gao, W., Zhang, P., Ye, Y., and Wei, Z., "Effects study of injection strategies on hydrogen-air formation and performance of hydrogen direct injection internal combustion engine," *Int J Hydrogen Energy* 44(47):26000–26011, 2019. https://doi.org/10.1016/j.ijhydene.2019.08.055.
24. Dhyani, V. and Subramanian, K.A., "Fundamental characterization of backfire in a hydrogen fuelled spark ignition engine using CFD and experiments," *Int J Hydrogen Energy* 44(60):32254–32270, 2019. https://doi.org/10.1016/j.ijhydene.2019.10.077.
25. Keck, M., Bessey, D., Buehler, F., Manuel, D., and Faiß, E., "Hydrogen Storage Technologies."
26. Ringler, J., Gerbig, F., Eichlseder, H., Wallner, T., "Insights into the development of a hydrogen combustion process with internal mixture formation," *Proceedings of the Sixth International Symposium on Internal combustion engine diagnostics*, 290–304, 2004.
27. Scarcelli, R., Kastengren, A.L., Powell, C.F., Wallner, T., and Matthias, N.S., "High-pressure gaseous injection: A comprehensive analysis of gas dynamics and mixing effects," *ASME 2012 Internal Combustion Engine Division Fall Technical Conference, ICEF 2012* 793–801, 2012. https://doi.org/10.1115/ICEF2012-92137.
28. Scarcelli, R., Wallner, T., Matthias, N., Salazar, V., and Kaiser, S., "Mixture Formation in Direct Injection Hydrogen Engines: CFD and Optical Analysis of Single-and Multi-Hole Nozzles," *Source: SAE International Journal of Engines* 4(2):2361–2375, 2011. https://doi.org/10.2307/26278302.
29. Battista, D. Di, Bartolomeo, M. Di, Villante, C., and Cipollone, R., "On the limiting factors of the waste heat recovery via ORC-based power units for on-the-road transportation sector," *Energy Convers Manag* 155:68–77, 2018. https://doi.org/10.1016/j.enconman.2017.10.091.
30. Väliheikki, A., Petallidou, K.C., Kalamaras, C.M., Kolli, T., Huuhtanen, M., Maunula, T., Keiski, R.L., and Efstathiou, A.M., "Selective catalytic reduction of NOx by hydrogen (H2-SCR) on WOx-promoted CezZr1-zO2 solids," *Appl Catal B* 156–157:72–83, 2014. https://doi.org/10.1016/j.apcatb.2014.03.008.
31. Hegde, B., Ahmed, Q., and Rizzoni, G., "Velocity and energy trajectory prediction of electrified powertrain for look ahead control," *Appl Energy* 279, 2020. https://doi.org/10.1016/j.apenergy.2020.115903.
32. Vassallo, A., Pesce, F., Arpaia, A., Millo, F., Rolando, L., Piano, A., and Bianco, A., "Ultra-lean Combustion System Optimization for H2-fuelled ICEs via Synergistic Application of 1D- and 3D-CFD," *SIA POWERTRAIN & POWER ELECTRONICS, Digital Edition 2021*, 1–9.
33. ZeEUS eBus Report #2 An updated overview of electric buses in Europe.
34. Ayman M. EL-Refaie, "Electrical Machines for Traction and Propulsion Applications," *Transportation Electrification: Breakthroughs in Electrified Vehicles, Aircraft, Rolling Stock, and Watercraft* , 1–26, 2023.
35. Shaobo, X., Qiankun, Z., Xiaosong, H., Yonggang, L., and Xianke, L., "Battery sizing for plug-in hybrid electric buses considering variable route lengths," *Energy* 226, 2021. https://doi.org/10.1016/j.energy.2021.120368.
36. Carlsson, L.-O. et al., "High-performance Battery for Premium Class Hybrid Vehicles," *MTZ Worldwide* 82(9):28–35, 2021.
37. Ager-Wick Ellingsen, L., Jayne Thorne, R., Wind, J., Figenbaum, E., Romare, M., and Nordelöf, A., "Life cycle assessment of battery electric buses," *Transp Res D Transp Environ* 112, 2022. https://doi.org/10.1016/j.trd.2022.103498.
38. Nanophosphate® high power lithiumion cell, 2023.
39. Rahantamialisoa, F.N.Z., Zembi, J., Miliozzi, A., Sahranavardfard, N., and Battistoni, M., "CFD simulations of under-expanded hydrogen jets under high-pressure injection conditions," *Journal of Physics: Conference Series*, Institute of Physics, 2022. https://doi.org/10.1088/1742-6596/2385/1/012051.
40. Duronio, F., Ranieri, S., Mascio, A. Di, and Vita, A. De, "Simulation of high pressure, direct injection processes of gaseous fuels by a density-based OpenFOAM solver," *Physics of Fluids* 33(6), 2021. https://doi.org/10.1063/5.0054098.
41. Rahantamialisoa, F., Battistoni, M., Miliozzi, A., Sahranavardfard, N., and Zembi, J., "Investigations on Hydrogen Injections Using a Real-Fluid Approach," *SAE Technical Paper 2023-01-0312, 2023. https://doi.org/10.4271/2023-01-0312.*
42. Panda, J. and Seasholtz, R.G., "Measurement of shock structure and shock-vortex interaction in underexpanded jets using Rayleigh scattering," *Physics of Fluids* 11(12):3761–3777, 1999. https://doi.org/10.1063/1.870247.

43. Hamzehloo, A. and Aleiferis, P.G., "LES and RANS modelling of under-expanded jets with application to gaseous fuel direct injection for advanced propulsion systems," *Int J Heat Fluid Flow* 76:309–334, 2019. https://doi.org/10.1016/j.ijheatfluidflow.2019.01.017.
44. Engine Combustion Network (ECN).
45. Salazar, V. and Kaiser, S., "Interaction of intake-induced flow and injection jet in a direct-injection hydrogen-fueled engine measured by PIV," *SAE 2011 World Congress and Exhibition*, 2011. https://doi.org/10.4271/2011-01-0673.
46. Ó Conaire, M., Curran, H.J., Simmie, J.M., Pitz, W.J., and Westbrook, C.K., "A comprehensive modeling study of hydrogen oxidation," *Int J Chem Kinet* 36(11):603–622, 2004. https://doi.org/10.1002/kin.20036.
47. Battista, D. Di, Bartolomeo, M. Di, and Cipollone, R., "Flow and thermal management of engine intake air for fuel and emissions saving," *Energy Convers Manag* 173:46–55, 2018. https://doi.org/10.1016/j.enconman.2018.07.074.
48. Dickes, R., Dumont, O., Legros, A., Quoilin, S., and Lemort, V., "Analysis and comparison of different modeling approaches for the simulation of a micro-scale organic Rankine cycle power plant," *Proceedings of ASME -ORC 2015* (October), 2015.
49. Legros, A., Guillaume, L., Diny, M., and Lemort, V., "Modelling, sizing and testing a scroll expander for a waste heat recovery application on a gasoline engine," *IOP Conf Ser Mater Sci Eng* 90(1), 2015. https://doi.org/10.1088/1757-899X/90/1/012065.
50. Fatigati, F., Bartolomeo, M. Di, Battista, D. Di, and Cipollone, R., "Experimental characterization of a hermetic scroll expander operating in an ORC-based power unit bottoming an internal combustion engine," *AIP Conf Proc* 2191(June 2016), 2019. https://doi.org/10.1063/1.5138802.
51. Fatigati, F., Vittorini, D., Coletta, A., and Cipollone, R., "Assessment of the differential impact of scroll and sliding vane rotary expander permeability on the energy performance of a small-scale solar-ORC unit," *Energy Convers Manag* 269:116169, 2022. https://doi.org/10.1016/j.enconman.2022.116169.
52. Marchionni, M., Fatigati, F., Bartolomeo, M. Di, Battista, D. Di, and Petrollese, M., "Experimental and Numerical Dynamic Investigation of an ORC System for Waste Heat Recovery Applications in Transportation Sector," *Energies* 15(24), 2022. https://doi.org/10.3390/en15249339.
53. Battista, D. Di and Cipollone, R., "Waste Energy Recovery and Valorization in Internal Combustion Engines for Transportation," *Energies* 16(8), 2023. https://doi.org/10.3390/en16083503.
54. Battista D., Di, Diomede D., Di, Prospero F., Di, Bartolomeo M., Di, Cipollone R., and Carapellucci R., "Turbocompound energy recovery option on a turbocharged diesel engine," *Italian thermal machines conference, Carpi, Modena*, 2023.
55. Battista, D. Di, Carapellucci, R., and Cipollone, R., "Integrated evaluation of Inverted Brayton cycle recovery unit bottomed to a turbocharged diesel engine," *Appl Therm Eng* 17:115353, 2020. https://doi.org/10.1016/j.applthermaleng.2020.115353.
56. Shi, M., Wang, H., Yang, C., Wang, Y., and Niu, X., "Experimental Research on the Matching Characteristics of the Compound VGT-STC System with a V-Type Diesel Engine," *Machines* 10(9), 2022. https://doi.org/10.3390/machines10090788.
57. Battista, D. Di, Bartolomeo, M. Di, and Cipollone, R., "Full energy recovery from exhaust gases in a turbocharged diesel engine," *Energy Convers Manag* 271(October):116280, 2022. https://doi.org/10.1016/j.enconman.2022.116280.
58. Bartolomeo, M. Di and Battista, D. Di, "Direct and Indirect Exhaust Heat Recovery from Turbocharged Heavy-Duty Engine," 2023. https://doi.org/10.4271/2023-24-0122
59. Savva, Z., Petallidou, K.C., Damaskinos, C.M., Olympiou, G.G., Stathopoulos, V.N., and Efstathiou, A.M., "H2-SCR of NOx on low-SSA CeO2-supported Pd: The effect of Pd particle size," *Appl Catal A Gen* 615, 2021. https://doi.org/10.1016/j.apcata.2021.118062.
60. Nanba, T., Kohno, C., Masukawa, S., Uchisawa, J., Nakayama, N., and Obuchi, A., "Improvements in the N2 selectivity of Pt catalysts in the NO-H2-O2 reaction at low temperatures," *Appl Catal B* 46(2):353–364, 2003. https://doi.org/10.1016/S0926-3373(03)00227-3.
61. Granger, P., Dhainaut, F., Pietrzik, S., Malfoy, P., Mamede, A.S., Leclercq, L., and Leclercq, G., "An overview: Comparative kinetic behaviour of Pt, Rh and Pd in the NO+CO and NO+H2 reactions," *Top Catal* 39(1–2):65–76, 2006. https://doi.org/10.1007/s11244-006-0039-0.

62. Zheng, L., Casapu, M., Stehle, M., Deutschmann, O., and Grunwaldt, J.D., "Selective Catalytic Reduction of NO x with Ammonia and Hydrocarbon Oxidation Over V 2 O 5 –MoO 3 /TiO 2 and V 2 O 5 –WO 3 /TiO 2 SCR Catalysts," *Top Catal* 62(1–4):129–139, 2019. https://doi.org/10.1007/s11244-018-1097-9.
63. Lang, W., Laing, P., Cheng, Y., Hubbard, C., and Harold, M.P., "Co-oxidation of CO and propylene on Pd/CeO2-ZrO2 and Pd/Al2O3 monolith catalysts: A light-off, kinetics, and mechanistic study," *Appl Catal B* 218:430–442, 2017. https://doi.org/10.1016/j.apcatb.2017.06.064.
64. Sheng, L., Ma, Z., Chen, S., Lou, J., Li, C., Li, S., Zhang, Z., Wang, Y., and Yang, H., "Mechanistic insight into N 2 O formation during NO reduction by NH 3 over Pd/CeO 2 catalyst in the absence of O 2," 2019.
65. Zhang, Q., Geng, G.N., Wang, S.W., Richter, A., and He, K. Bin, "Satellite remote sensing of changes in NO x emissions over China during 1996-2010," *Chinese Science Bulletin* 57(22):2857–2864, 2012. https://doi.org/10.1007/s11434-012-5015-4.
66. Khoder, M.I., "Atmospheric conversion of sulfur dioxide to particulate sulfate and nitrogen dioxide to particulate nitrate and gaseous nitric acid in an urban area."
67. Liberzon, D., "Calculus of variations and optimal control theory: a concise introduction," 2011.
68. Onori, S., Serrao, L., and Rizzoni, G., "Hybrid electric vehicles: Energy management strategies," 2016.
69. Donatantonio, F., Ferrara, A., Polverino, P., Arsie, I., and Pianese, C., "Novel Approaches for Energy Management Strategies of Hybrid Electric Vehicles and Comparison with Conventional Solutions," *Energies* 15(6), 2022. https://doi.org/10.3390/en15061972.